

$\text{Y}_{2-x-y}\text{Bi}_x\text{Eu}_y\text{MgTiO}_6$ 荧光粉的发光特性研究

刘昊¹ 熊正烨¹ 曾才兴¹ 张泽峰¹ 塞辰茜² 郭竞渊¹

1(广东海洋大学 电子与信息工程学院 湛江 524088)

2(广东海洋大学 化学与环境学院 湛江 524088)

摘要 双钙钛矿因其结构灵活、易于掺杂、热稳定性好等优点，成为近几年的研究热点。稀土掺杂双钙钛矿基质材料的光致发光研究常见报道，但和热释光有关的研究较少。本文采用高温固相法合成了 Bi^{3+} 和 Eu^{3+} 共掺的 $\text{Y}_{2-x-y}\text{Bi}_x\text{Eu}_y\text{MgTiO}_6$ ($0 \leq x < 1, 0 \leq y < 1$)系列样品，并测量了样品的X射线衍射谱(X-ray Diffraction, XRD)、光致发光光谱(Photoluminescence, PL)和热释光谱(Thermoluminescence, TL)。XRD分析表明：样品的晶体结构均为单斜晶系 $\text{P}2_1/\text{n}$ ， Bi^{3+} 和 Eu^{3+} 通过替代 Y^{3+} 而掺入 Y_2MgTiO_6 中；PL表明：样品最佳掺杂浓度为 $x=0.01, y=0.20$ ，该样品在620 nm附近有较强的红光发射(对应 Eu^{3+} 的 $^5\text{D}_0 \rightarrow ^7\text{F}_2$ 跃迁)，并伴有长余辉；测定不同浓度 Bi^{3+} 和 Eu^{3+} 掺杂样品的TL曲线也观察到 $\text{Y}_{1.79}\text{Bi}_{0.01}\text{Eu}_{0.20}\text{MgTiO}_6$ 的热释光灵敏度最高，样品在510 K和610 K附近有两个显著的TL峰；热释光谱比荧光谱更为丰富， Eu^{3+} 的 $^5\text{D}_0 \rightarrow ^7\text{F}_J$ ($J=1, 2, 3, 4$)跃迁均可被观测到，样品的TL光强与辐照剂量在2~1 000 Gy范围内具有良好的线性关系。采用不同预热温度(T_m-T_{stop})和计算机拟合(Glow Curve Deconvolution, GCD)两种方法分析样品的TL动力学参数，发现样品中热释光陷阱深度从0.80 eV延伸到1.40 eV。上述测试和分析结果表明：热释光谱比荧光谱更为丰富； $\text{Y}_{1.79}\text{Bi}_{0.01}\text{Eu}_{0.20}\text{MgTiO}_6$ 荧光粉可作为大剂量检测的热释光剂量计材料。

关键词 Y_2MgTiO_6 ，稀土掺杂，光致发光，热释光，激活能

中图分类号 TL271, TL818

DOI: [10.11889/j.0253-3219.2023.hjs.46.060501](https://doi.org/10.11889/j.0253-3219.2023.hjs.46.060501)

Luminescence characteristics of $\text{Y}_{2-x-y}\text{Bi}_x\text{Eu}_y\text{MgTiO}_6$ phosphors

LIU Hao¹ XIONG Zhengye¹ ZENG Caixing¹ ZHANG Zefeng¹ JIAN Chenxi² GUO Jingyuan¹

1(School of Electronics and Information Engineering, Guangdong Ocean University, Zhanjiang 524088, China)

2(School of Chemistry and Environment, Guangdong Ocean University, Zhanjiang 524088, China)

Abstract [Background] Double perovskites have become a research hotspot in recent years due to their flexible structure, easy doping, and good thermal stability. Photoluminescence (PL) of rare-earth-doped double perovskite materials has been frequently reported, but few studies on thermoluminescence (TL) have been conducted. [Purpose] This study aims to investigate the TL characteristics of $\text{Y}_{2-x-y}\text{Bi}_x\text{Eu}_y\text{MgTiO}_6$ ($0 \leq x < 1, 0 \leq y < 1$) phosphors. [Method] Bi^{3+} and Eu^{3+} co-doped Y_2MgTiO_6 samples were synthesized by a high-temperature solid phase method, and the X-ray diffraction (XRD), PL, and TL of the samples were measured. [Results] XRD analysis results show that the crystal structures of all samples are monoclinic $\text{P}2_1/\text{n}$, and Bi^{3+} and Eu^{3+} are doped into Y_2MgTiO_6 by substituting Y^{3+} . The PL results show that $\text{Y}_{1.79}\text{Bi}_{0.01}\text{Eu}_{0.20}\text{MgTiO}_6$ has a strong red emission near 620 nm (corresponding to the $^5\text{D}_0 \rightarrow ^7\text{F}_2$

广东省科技计划(No.2015A020216020)、广东海洋大学科研项目(No.060302112102)资助

第一作者：刘昊，男，2000年出生，2021年毕业于山东工商学院，现为硕士研究生，研究领域为稀土发光材料

通信作者：郭竞渊，E-mail: gjy3344@126.com

收稿日期：2022-12-30，修回日期：2023-02-26

Supported by Guangdong Science and Technology Plan (No.2015A020216020), Guangdong Ocean University Research Project (No.060302112102)

First author: LIU Hao, male, born in 2000, graduated from Shandong Technology and Business University in 2021, master student, focusing on rare earth luminescent materials

Corresponding author: GUO Jingyuan, E-mail: gjy3344@126.com

Received date: 2022-12-30, revised date: 2023-02-26

transition of Eu^{3+}), which is accompanied by a long afterglow. The TL curves of the samples doped with different concentrations of Bi and Eu ions show that $\text{Y}_{1.79}\text{Bi}_{0.01}\text{Eu}_{0.20}\text{MgTiO}_6$ has the highest TL sensitivity, and the samples exhibits two significant TL peaks near 510 K and 610 K. The TL spectrum is more abundant than the fluorescence spectrum, and the $^5\text{D}_0 \rightarrow ^7\text{F}_J$ ($J=1,2,3,4$) transition of Eu^{3+} can be observed. The TL intensity of the sample has a good linear relationship with the irradiation dose in the range of 2~1 000 Gy. The TL kinetic parameters of the samples are analyzed using two methods under different preheating temperatures (T_m and T_{stop}) and glow curve deconvolution. The analysis results show that the depth of the TL trap in the sample extends from 0.80 eV to 1.40 eV. [Conclusions] The results of this study indicate that the TL spectrum is richer than the PL spectrum and that $\text{Y}_{1.79}\text{Bi}_{0.01}\text{Eu}_{0.20}\text{MgTiO}_6$ may be used as TL dosimeter material for large dose detection.

Key words Y_2MgTiO_6 , Rare-earth doping, Photoluminescence, Thermoluminescence, Activation energy

研究表明,掺杂稀土离子的氧化物基质材料可能有利于提高光学和剂量学性能^[1~5],氧化物基质材料中,双钙钛矿因具有极好的化学结构和良好的稳定性被广泛关注^[6]。用不同的A'或B'离子部分取代 ABO_3 型简单钙钛矿的A或B位可得到AA'BB'O₆型双钙钛矿。双钙钛矿作为新型基质材料,其结构和发光性能已有较广泛的研究,如 $\text{La}_2\text{MgTiO}_6$ ^[7]、 $\text{Gd}_2\text{ZnTiO}_6$ ^[8]、 La_2MTiO_6 (M=Co,Ni)^[9]具有良好的热稳定性和优越的发光性能,可作为照明领域的候选材料。 Y_2MgTiO_6 基质材料因其物化性稳定、易于制备、原材料来源广泛成为近几年的研究热点^[10]。

热释光材料中含有一定浓度的发光中心和陷阱,在高能射线激发下,晶体内部会产生自由电子和空穴,其中一部分电子(或空穴)被陷阱俘获;晶体受热升温时,被俘获的电子(或空穴)受热激发成为近自由载流子,近自由载流子与发光中心复合时就产生热释光^[11~12]。对热释光发光曲线进行分析可估计陷阱的种类和激活能等信息^[13~16]。很多热释光材料因其剂量响应的线性较好、易于制造、成本低^[17~19],可用于电离辐射剂量检测,如LiF:Mg,Cu,P^[20]、 $\text{Li}_2\text{B}_4\text{O}_7:\text{Mn}$ ^[21]可用于个人剂量检测;BeO^[22]、 $\text{CaSO}_4:\text{Dy}$ ^[23]、 $\text{CaF}_2:\text{Dy}$ ^[24]可用于环境剂量检测; $\text{Al}_2\text{O}_3:\text{C}$ ^[25]、 $\text{MgB}_4\text{O}_7:\text{Dy}$ ^[26]可应用于医疗剂量检测。除标准的热释光剂量计外,还有其他可能用于剂量检测的材料,如SrGd₂O₄:Sm³⁺、SrDy₂O₄:Eu³⁺、BaSi₂O₅:Dy³⁺、(Sr,Ba)AlO₄:Eu²⁺/Dy³⁺、CaWO₄:Pr³⁺、LaGa₄O₇(BO₃)₃和(Ba,Sr)TiO₃:Pr³⁺等^[27~35]。一般的热释光剂量计灵敏度较高,但剂量响应的线性上限一般都不太高(约200 Gy)^[36]。在一些特殊场合(如辐照保鲜领域)常需准确测量kGy级的辐照剂量^[37~38]。因此,研究性能稳定、剂量响应线性范围较宽的热释光材料可拓展热释光技术的应用领域。

采用高温固相法研制了Bi³⁺和Eu³⁺共掺的 Y_2MgTiO_6 (简称YMT)荧光粉,并测量YMT的X射线衍射谱(X-ray Diffraction,XRD)、光致发光光谱

(Photoluminescence, PL) 和热释光(Thermoluminescence, TL),研究其用作大剂量场合热释光剂量计材料的可能性。

1 实验方法

1.1 样品制备

采用高温固相法合成 $\text{Y}_{2-x-y}\text{Bi}_x\text{Eu}_y\text{MgTiO}_6$ ($x=0$ 、0.001、0.002、0.005、0.010、0.020、0.050、0.100, $y=0$ 、0.05、0.10、0.15、0.20、0.25、0.30)系列荧光粉。按照化学计量比称取一定量的 Y_2O_3 (99.99%)、 MgO (99.99%)、 TiO_2 (99.99%)、 Bi_2O_3 (99.99%)和 Eu_2O_3 (99.99%)置于玛瑙研钵中,充分研磨0.5 h至混合均匀,将研磨均匀的粉末置于刚玉坩埚中并放置在马弗炉内,在空气氛围下升温至800 °C预烧3 h,然后快速升温至1 300 °C煅烧9 h,得到块状的烧结样品,将块状样品用玛瑙研钵压碎研磨得到荧光粉体。

采用日本理学Ultima IV型X射线衍射仪测量不同样品的XRD,测量时使用Cu-K α 辐射源,扫描范围为10°~80°,扫描速率为5 (°)·min⁻¹,结果如图1所示。无机晶体信息数据库中缺少 Y_2MgTiO_6 的信息,Shannon^[39]采用Rietveld方法对数据进行了分析,得出的结果证明 $\text{Dy}_2\text{MgTiO}_6$ 和 Y_2MgTiO_6 具有类似的结构,因此,使用 $\text{Dy}_2\text{MgTiO}_6$ 的标准卡作为参考。由图1可知,不同样品的XRD峰的数量和位置与标准卡(ICDD 04-021-1637)的衍射峰基本一致,说明合成样品的晶体结构均为单斜晶系P2₁/n, Bi³⁺和Eu³⁺的引入不会产生其他杂质相的衍射峰。因Bi³⁺和Eu³⁺的离子半径和电荷构型与Y³⁺基本一致,故Bi³⁺和Eu³⁺通过替代Y³⁺的位置掺入 Y_2MgTiO_6 中^[40]。

1.2 测量方法

采用HITACHI F-7000荧光光谱仪测量样品的光致发光光谱,激发光源为Xe灯,光谱分辨率为0.2 nm。采用英国爱丁堡公司生产的FSP920稳态/

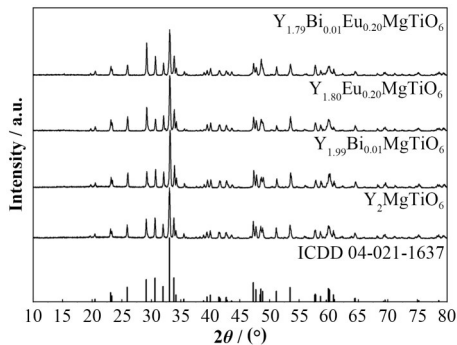


图1 $\text{Y}_{2-x-y}\text{Bi}_x\text{Eu}_y\text{MgTiO}_6$ 荧光粉的XRD图谱
Fig.1 XRD patterns of $\text{Y}_{2-x-y}\text{Bi}_x\text{Eu}_y\text{MgTiO}_6$ phosphors

瞬态荧光光谱仪测量样品的荧光寿命曲线,时间扫描步长为1 s。采用LTTL3DS热释光谱仪(广州瑞迪科技有限公司)对样品进行辐照和热释光谱(TL3D)的测量,辐照源为X光管,X光管的工作电压为50 kV,电流为150 μA ,剂量率约为0.1 $\text{Gy}\cdot\text{s}^{-1}$,测量时升温速率为5 $\text{K}\cdot\text{s}^{-1}$,升温区间为300~750 K。采用Risø TL/OSL-15-B/C热释光/光释光测量仪对样品进行辐照和热释光曲线的测量,辐照源为仪器配备的⁹⁰Srβ放射源,剂量率约为0.1 $\text{Gy}\cdot\text{s}^{-1}$ 。

2 结果与讨论

2.1 光致发光光谱分析

为探究样品掺杂离子浓度与发光强度的关系,测量了 $\text{Y}_{2-x-y}\text{Bi}_x\text{Eu}_y\text{MgTiO}_6$ 系列样品的发射光谱($\lambda_{\text{ex}}=398 \text{ nm}$),结果如图2所示。由图2可知,所有样品的PL中都存在4个发光峰,分别位于560 nm、593 nm、600 nm和620 nm。其中,620 nm处的发光峰对应 Eu^{3+} 的 $^5\text{D}_0 \rightarrow ^7\text{F}_2$ 跃迁。560 nm、593 nm、600 nm处的三个发光峰对应 Eu^{3+} 的 $^5\text{D}_0 \rightarrow ^7\text{F}_1$ 跃迁(离子半径较大的 Eu^{3+} 替代 Y^{3+} 时, Eu-O 键缩短导致晶格畸变,晶体对称性降低, Eu^{3+} 的 $^7\text{F}_1$ 能级解除简并,劈裂为3个能级)^[41]。从图2(a)中可以观察到,随着 Eu^{3+} 掺杂浓度($y < 0.20$)的增加,发射光谱强度逐渐增强;当 y 大约0.20时,发射光谱强度最大;随着 Eu^{3+} 掺杂浓度的进一步增加会导致发射光谱强度明显下降,即产生浓度猝灭效应。由图2(b)可知,Bi³⁺掺杂浓度的增加会增强 Eu^{3+} 的特征发光,且Bi³⁺最佳掺杂浓度约为0.01,当掺杂浓度大于0.01后也会产生浓度猝灭效应。由此可见 $\text{Y}_{1.79}\text{Bi}_{0.01}\text{Eu}_{0.20}\text{MgTiO}_6$ 为最佳样品。

2.2 荧光寿命曲线分析

荧光粉晶格缺陷所导致的电子俘获中心是影响余辉发光的持续时间和亮度的决定性因素^[42]。实验使用254 nm的紫外光灯照射 $\text{Y}_{1.79}\text{Bi}_{0.01}\text{Eu}_{0.20}\text{MgTiO}_6$

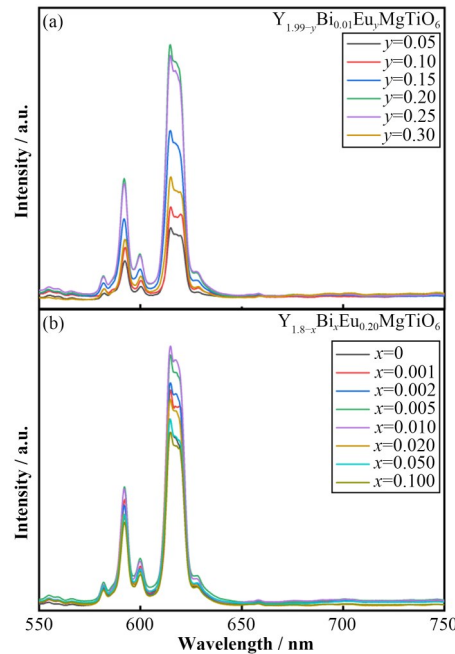


图2 398 nm激发下 $\text{Y}_{1.99-y}\text{Bi}_{0.01}\text{Eu}_y\text{MgTiO}_6$ 荧光粉(a)和 $\text{Y}_{1.8-x}\text{Bi}_x\text{Eu}_{0.20}\text{MgTiO}_6$ 荧光粉(b)的发射光谱(彩图见网络版)
Fig.2 Emission spectra of $\text{Y}_{1.99-y}\text{Bi}_{0.01}\text{Eu}_y\text{MgTiO}_6$ phosphors (a) and $\text{Y}_{1.8-x}\text{Bi}_x\text{Eu}_{0.20}\text{MgTiO}_6$ phosphors (b) under 398-nm excitation (color online)

样品300 s,确保晶体中电子俘获中心的俘获电子近似饱和,然后关闭激发源并测量荧光寿命曲线,结果如图3(a)所示。样品的荧光寿命曲线可被双指数函数很好拟合:

$$I_t = A_1 \exp(t/\tau_1) + A_2 \exp(t/\tau_2) \quad (1)$$

式中: I_t 为发光强度; A_1 、 A_2 为常数; t 为时间; τ 为衰减寿命。拟合结果中 τ_1 和 τ_2 的值分别为0.59 s和5.50 s。 τ 值均大于0.1 s,说明样品伴有长余辉,且可能存在激活能较小的载流子俘获中心。由荧光寿命曲线符合式(2)^[43],并由此可判断俘获中心中激发的载流子被再次俘获的可能性:

$$I_t = \frac{I_0}{(1 + \frac{t}{\tau})^{b/(b-1)}} \quad (2)$$

式中: b 为动力学阶数,可以反映体系中陷阱的再俘获过程。分别对快衰退曲线和慢衰退曲线进行拟合,结果如图3(b)和(c)所示,拟合后的曲线斜率分别为 $b/(1-b)$ 。由图3可知,拟合后曲线的斜率分别为-3.57和-2.62,可算出动力学阶数 b 值分别为1.39和1.62,表明体系中陷阱的再俘获过程不可忽略。

2.3 TL分析

2.3.1 掺杂浓度优化

TL测试样品质量均为25 mg,测试步骤如下:将样品预热至773 K保持10 s;冷却至室温后使用⁹⁰Sr

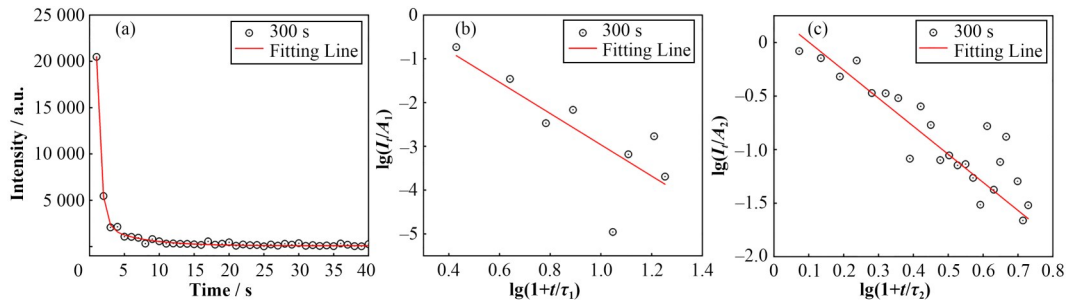


图3 $\text{Y}_{1.79}\text{Bi}_{0.01}\text{Eu}_{0.20}\text{MgTiO}_6$ 荧光粉的荧光寿命曲线(a)、快衰退拟合曲线(b)和慢衰退拟合曲线(c)
Fig.3 Fluorescence lifetime curve (a), fast decay fitting curve (b), and slow decay fitting curve (c) of $\text{Y}_{1.79}\text{Bi}_{0.01}\text{Eu}_{0.20}\text{MgTiO}_6$ phosphors

β 放射源辐照 80 Gy 后, 测量 TL(升温速率为 $5 \text{ K} \cdot \text{s}^{-1}$)。测量结果如图 4 所示。图 4(a)为 $\text{Y}_{1.99-y}\text{Bi}_{0.01}\text{Eu}_y\text{MgTiO}_6$ ($y=0, 0.05, 0.10, 0.15, 0.20, 0.25$) 样品的 TL, 图 4(a)中插图为 TL 积分强度随 Eu^{3+} 掺杂浓度变化的归一化面积曲线。图 4(b)为 $\text{Y}_{1.8-x}\text{Bi}_x\text{Eu}_{0.2}\text{MgTiO}_6$ ($x=0.005, 0.01, 0.02, 0.05, 0.10$) 样品的 TL, 图 4(b)中插图为 TL 积分强度随 Bi^{3+} 掺杂浓度变化的归一化面积曲线。由图 4 可知, 样品的热释光峰较宽, 随着掺杂离子浓度的变化热释光峰位置没有明显改变, 说明掺杂离子浓度变化对样品中的陷阱深度的影响较小, $\text{Y}_{1.79}\text{Bi}_{0.01}\text{Eu}_{0.20}\text{MgTiO}_6$ 为热释光灵敏度最高的样品。

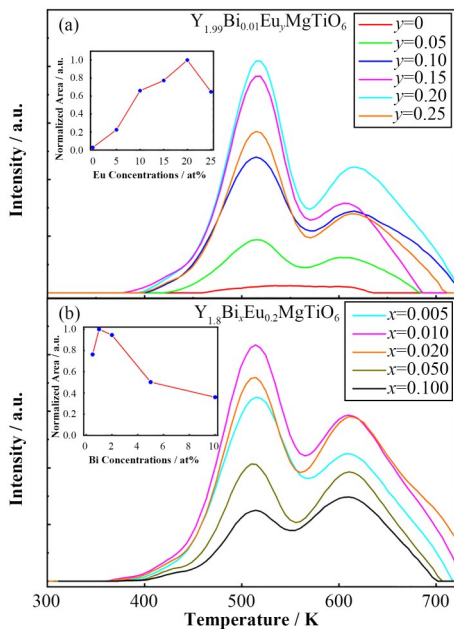


图4 $\text{Y}_{1.99-y}\text{Bi}_{0.01}\text{Eu}_y\text{MgTiO}_6$ 荧光粉(a)和 $\text{Y}_{1.8-x}\text{Bi}_x\text{Eu}_{0.2}\text{MgTiO}_6$ 荧光粉(b)的热释光曲线
Fig.4 TL curves of $\text{Y}_{1.99-y}\text{Bi}_{0.01}\text{Eu}_y\text{MgTiO}_6$ phosphors (a) and $\text{Y}_{1.8-x}\text{Bi}_x\text{Eu}_{0.2}\text{MgTiO}_6$ phosphors (b)

样品的 3D-TL 测试步骤如下: 将样品预热至 773 K 保持 10 s; 待冷却至室温后使用 X 射线辐照 80 Gy 后, 测量 TL3D(升温速率为 $5 \text{ K} \cdot \text{s}^{-1}$), 结果如

图 5 所示。由图 5 可知, $\text{Y}_{1.79}\text{Bi}_{0.01}\text{Eu}_{0.20}\text{MgTiO}_6$ 样品的热释光谱比 PL 光谱更丰富, 不仅看到 Eu^{3+} 在 590 nm 和 620 nm 处的特征发射, 还可以观测到 Eu^{3+} 在 650 nm($^5\text{D}_0 \rightarrow ^7\text{F}_3$) 和 700 nm($^5\text{D}_0 \rightarrow ^7\text{F}_4$) 左右的特征发射。TL3D 中 620 nm 和 700 nm 处的发射强度较强, 其他跃迁的发射强度相对较弱, 且在 510 K 和 610 K 左右存在明显的热释光峰。上述现象说明 Eu^{3+} 为样品的发光中心, Eu^{3+} 的 $^5\text{D}_0 \rightarrow ^7\text{F}_2$, $^5\text{D}_0 \rightarrow ^7\text{F}_4$ 两种能级跃迁释放光子为主要的发光方式。

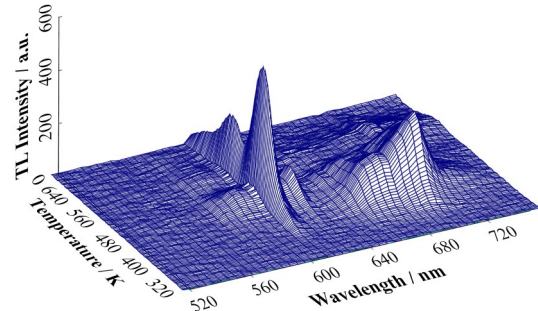


图5 $\text{Y}_{1.79}\text{Bi}_{0.01}\text{Eu}_{0.20}\text{MgTiO}_6$ 荧光粉的三维热释光谱
Fig.5 TL 3D spectra of $\text{Y}_{1.79}\text{Bi}_{0.01}\text{Eu}_{0.20}\text{MgTiO}_6$ phosphors

2.3.2 剂量响应

$\text{Y}_{1.79}\text{Bi}_{0.01}\text{Eu}_{0.20}\text{MgTiO}_6$ 样品 TL 剂量响应测试在 Risø TL/OSL-15-B/C 上完成, ${}^{90}\text{Sr}$ β 放射源的放射性活度为 1.4 GBq, ${}^{90}\text{Sr}$ β 放射源与样品的距离为 5 mm, 探测器与样品的距离为 55 mm。测试步骤如下: 将样品预热至 773 K 保持 10 s; 待冷却至室温后辐照 2 Gy 后, 测量 TL(升温速率为 $5 \text{ K} \cdot \text{s}^{-1}$)。重复以上步骤, 改变辐照剂量为 5 Gy、10 Gy、20 Gy、50 Gy、70 Gy、100 Gy、120 Gy、150 Gy、200 Gy、300 Gy、400 Gy、500 Gy、700 Gy、800 Gy、900 Gy、1 000 Gy, 再测量和记录 TL 发光曲线。记录 300~773 K 范围内 TL 曲线的积分强度, 作出剂量响应曲线, 如图 6 所示。图中每个实验点为 TL 曲线下的积分面积, 实线为实验点的线性拟合($y=(2.815 \pm 0.009)+(0.964 \pm 0.003)x$), 在测试范围内未出现饱和现象, 剂量响应

在2~1 000 Gy的范围内线性较好,线性范围较宽^[44~45]。该材料相较于常用的热释光剂量计有更高的饱和剂量,剂量响应约在1 kGy仍能保持良好线性,因此,该材料可作为热释光剂量计应用于大剂量场合,如辐照保鲜领域。

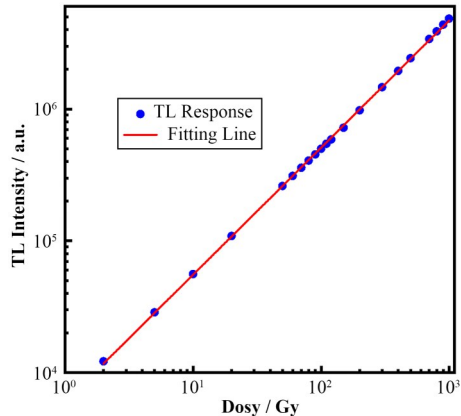


图6 $\text{Y}_{1.79}\text{Bi}_{0.01}\text{Eu}_{0.20}\text{MgTiO}_6$ 荧光粉的剂量响应曲线
Fig.6 Dose response curve of $\text{Y}_{1.79}\text{Bi}_{0.01}\text{Eu}_{0.20}\text{MgTiO}_6$ phosphors

2.3.3 计算机拟合

计算机拟合(Glow Curve Deconvolution, GCD)法广泛用于研究比较复杂的TL机制,可得出TL曲线中重叠峰的数量和各个峰的动力学参数。采用GCD法对使用⁹⁰Sr β放射源辐照80 Gy的 $\text{Y}_{1.79}\text{Bi}_{0.01}\text{Eu}_{0.20}\text{MgTiO}_6$ 样品的TL曲线进行拟合,曲线可用7个TL发光峰的叠加,每个发光峰都可用式(3)表示^[46],拟合曲线见图7,参数见表1。

$$I(t) = s n_0 \exp\left(-\frac{E}{kT}\right) \cdot [1 + \frac{s(b-1)}{\beta} \int_{T_0}^T \exp\left(-\frac{E}{kT'}\right) dT']^{\frac{b}{b-1}} \quad (3)$$

式中: n_0 是捕获电子在样品中的初始数目; E 是俘获电子的活化能,eV; s 是频率因子,Hz; k 是Boltzmann常数,即 0.862×10^{-4} eV·K⁻¹; β 是样品的加热速率,K·s⁻¹,在本实验中为5 K·s⁻¹; T 是以K为单位的绝对温度; b 是动力学级数。从图7可以看出,拟合曲线与实验点吻合得很好。

2.3.4 T_m-T_{stop} 法

为进一步确认动力学拟合的可靠性,使用 T_m-T_{stop} 方法进行验证^[47~48]。 T_m-T_{stop} 方法步骤如下:1)将之前辐照的样品加热到足够高的温度(T_{stop}),以读取几乎整个TL信号;2)将样品快速冷却到室温;3)以相同的加热速率重新加热样品,以记录剩余的TL曲线,并记下第一个TL极大值位置 T_m 。然后用稍低的 T_{stop} 值(约降低4 K)重复整个过程。图8给出了 T_m 与 T_{stop} 之间的关系图。每个成分的峰值位置与计算

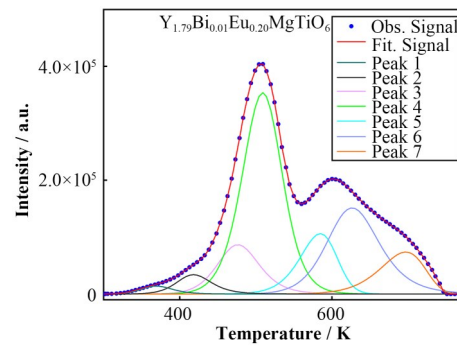


图7 80 Gy辐照剂量下 $\text{Y}_{1.79}\text{Bi}_{0.01}\text{Eu}_{0.20}\text{MgTiO}_6$ 荧光粉的TL曲线拟合

Fig.7 TL fitting curve of $\text{Y}_{1.79}\text{Bi}_{0.01}\text{Eu}_{0.20}\text{MgTiO}_6$ phosphors at 80-Gy irradiation dose

表1 GCD法分析得到 $\text{Y}_{1.79}\text{Bi}_{0.01}\text{Eu}_{0.20}\text{MgTiO}_6$ 荧光粉的动力学参数

Table 1 Kinetic parameters of $\text{Y}_{1.79}\text{Bi}_{0.01}\text{Eu}_{0.20}\text{MgTiO}_6$ phosphors obtained by the GCD method

动力学参数 Peaks	E / eV	$\text{Y}_{1.79}\text{Bi}_{0.01}\text{Eu}_{0.20}\text{MgTiO}_6$		
		T_m / K	b	s / s^{-1}
1	0.80	369	2.0	2.30×10^{10}
2	0.92	418	2.0	4.00×10^{10}
3	0.95	476	1.8	2.60×10^9
4	1.06	509	1.6	7.33×10^9
5	1.32	585	1.2	4.99×10^{10}
6	1.37	626	2.0	1.84×10^{10}
7	1.40	697	1.0	2.19×10^9

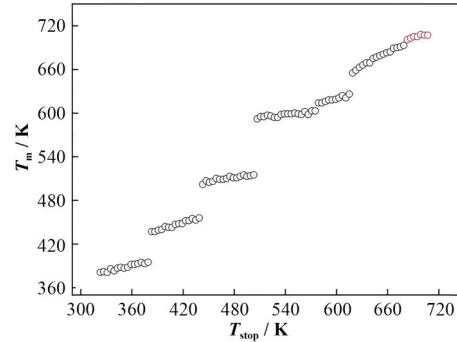


图8 $\text{Y}_{1.79}\text{Bi}_{0.01}\text{Eu}_{0.20}\text{MgTiO}_6$ 的 T_m-T_{stop} 图
Fig.8 Plot of T_m vs. T_{stop} of $\text{Y}_{1.79}\text{Bi}_{0.01}\text{Eu}_{0.20}\text{MgTiO}_6$

机拟合的结果基本一致。

3 结语

采用高温固相法合成 $\text{Y}_{2-x-y}\text{Bi}_x\text{Eu}_y\text{MgTiO}_6$ 系列红色发光材料,测量系列样品的PL和TL,得到最佳样品为 $\text{Y}_{1.79}\text{Bi}_{0.01}\text{Eu}_{0.20}\text{MgTiO}_6$ 。通过测量分析该样品的TL3D、剂量响应、TL曲线,可得到如下结果:

1)样品的发光中心为 Eu^{3+} 的相关缺陷;样品的3D-TL比PL更丰富,热释光谱不仅可观测到 Eu^{3+} 在

590 nm ($^5\text{D}_0 \rightarrow ^7\text{F}_1$) 和 620 nm ($^5\text{D}_0 \rightarrow ^7\text{F}_2$) 处的特征发光 (PL 可观测到), 还观察到 Eu³⁺ 在 650 nm ($^5\text{D}_0 \rightarrow ^7\text{F}_3$) 和 700 nm ($^5\text{D}_0 \rightarrow ^7\text{F}_4$) 处的特征发光 (PL 几乎观测不到)。

2) 实验测得 $\text{Y}_{1.79}\text{Bi}_{0.01}\text{Eu}_{0.2}\text{MgTiO}_6$ 样品的 TL 光强与辐照剂量在 2~1 000 Gy 范围内线性较好, 饱和剂量在 1 kGy 以上, 且该荧光粉热稳定性较好、制备成本低。该荧光粉可作为热释光剂量计应用于大剂量辐照场合, 如辐射保鲜领域。

3) 通过分析热释光发光曲线可知, 荧光粉在室温以上存在 7 个 TL 发光峰, 对应的载流子俘获中心的激活能分别为 0.80 eV、0.92 eV、0.95 eV、1.06 eV、1.32 eV、1.37 eV、1.40 eV, 这一结果与 T_m-T_{stop} 法分析的结果基本吻合。

作者贡献声明 刘昊负责实验方案的设计、数据分析、数据处理和论文撰写; 熊正烨提供理论指导和论文的完善意见; 曾才兴、张泽锋、蹇辰茜参与实验材料的制备; 郭竞渊提供理论指导和论文的数据分析。

参考文献

- 1 Singh J, Manam J. Effect of Y³⁺ on structural environment and luminescence characteristics of novel SrGd_{1.94-2x}Eu_{0.06}Y_{2x}O₄ phosphors for display and dosimetric applications[J]. Materials Research Bulletin, 2017, **88**: 105~113. DOI: [10.1016/j.materresbull.2016.12.024](https://doi.org/10.1016/j.materresbull.2016.12.024).
- 2 Gavhane K H, Bhadane M S, Kulkarni P P, et al. Investigation of novel Eu doped SrDy₂O₄ microphosphor for thermoluminescence dosimetry[J]. Journal of Luminescence, 2021, **231**: 117781. DOI: [10.1016/j.jlumin.2020.117781](https://doi.org/10.1016/j.jlumin.2020.117781).
- 3 Sarıkci S, Topaksu M, Bakr M, et al. Structural and analyses of thermoluminescence glow curves in Sm doped SrGd₂O₄ phosphor[J]. Journal of Alloys and Compounds, 2022, **911**: 165008. DOI: [10.1016/j.jallcom.2022.165008](https://doi.org/10.1016/j.jallcom.2022.165008).
- 4 Jin S L, Li R F, Huang H, et al. Compact ultrabroadband light-emitting diodes based on lanthanide-doped lead-free double perovskites[J]. Light: Science & Applications, 2022, **11**: 52. DOI: [10.1038/s41377-022-00739-2](https://doi.org/10.1038/s41377-022-00739-2).
- 5 Li X B, Liu Q, Huang W T, et al. Structural and luminescent properties of Eu³⁺-doped double perovskite BaLaMgNbO₆ phosphor[J]. Ceramics International, 2018, **44**(2): 1909~1915. DOI: [10.1016/j.ceramint.2017.10.130](https://doi.org/10.1016/j.ceramint.2017.10.130).
- 6 Khalfin S, Bekenstein Y. Advances in lead-free double perovskite nanocrystals, engineering band-gaps and enhancing stability through composition tunability[J]. Nanoscale, 2019, **11**(18): 8665~8679. DOI: [10.1039/c9nr01031a](https://doi.org/10.1039/c9nr01031a).
- 7 Chen Z M, Wang Z Y, Kang W D, et al. Preparation and luminescent properties of double perovskite-type La_{2-x-y}Y_xMgTiO₆: yEu³⁺ red fluorescent materials[J]. Journal of Luminescence, 2022, **243**: 118656. DOI: [10.1016/j.jlumin.2021.118656](https://doi.org/10.1016/j.jlumin.2021.118656).
- 8 Zheng T, Luo L H, Du P, et al. Highly-efficient double perovskite Mn⁴⁺-activated Gd₂ZnTiO₆ phosphors: a bifunctional optical sensing platform for luminescence thermometry and manometry[J]. Chemical Engineering Journal, 2022, **446**: 136839. DOI: [10.1016/j.cej.2022.136839](https://doi.org/10.1016/j.cej.2022.136839).
- 9 Rodríguez E, López M L, Campo J, et al. Crystal and magnetic structure of the perovskites La₂MTiO₆ (M=Co, Ni) [J]. Journal of Materials Chemistry, 2002, **12**(9): 2798~2802. DOI: [10.1039/B202504N](https://doi.org/10.1039/B202504N).
- 10 Li J Q, Liao J S, Wen H R, et al. Multiwavelength near infrared downshift and downconversion emission of Tm³⁺ in double perovskite Y₂MgTiO₆: Mn⁴⁺/Tm³⁺ phosphors via resonance energy transfer[J]. Journal of Luminescence, 2019, **213**: 356~363. DOI: [10.1016/j.jlumin.2019.05.038](https://doi.org/10.1016/j.jlumin.2019.05.038).
- 11 Xu J, Tanabe S. Persistent luminescence instead of phosphorescence: history, mechanism, and perspective[J]. Journal of Luminescence, 2019, **205**: 581~620. DOI: [10.1016/j.jlumin.2018.09.047](https://doi.org/10.1016/j.jlumin.2018.09.047).
- 12 Gupta K K, Kadam R M, Dhoble N S, et al. Photoluminescence, thermoluminescence and evaluation of some parameters of Dy³⁺ activated Sr₅(PO₄)₃F phosphor synthesized by sol-gel method[J]. Journal of Alloys and Compounds, 2016, **688**: 982~993. DOI: [10.1016/j.jallcom.2016.07.114](https://doi.org/10.1016/j.jallcom.2016.07.114).
- 13 Kadam A R, Mishra G C, Dhoble S J. Thermoluminescence study and evaluation of trapping parameters CaTiO₃: RE (RE=Eu³⁺, Dy³⁺) phosphor for TLD applications[J]. Journal of Molecular Structure, 2021, **1225**: 129129. DOI: [10.1016/j.molstruc.2020.129129](https://doi.org/10.1016/j.molstruc.2020.129129).
- 14 Kitis G, Pagonis V. On the resolution of overlapping peaks in complex thermoluminescence glow curves[J]. Nuclear Instruments and Methods in Physics Research Section A: Accelerators, Spectrometers, Detectors and Associated Equipment, 2019, **913**: 78~84. DOI: [10.1016/j.nima.2018.10.056](https://doi.org/10.1016/j.nima.2018.10.056).
- 15 Sadek A M, Kitis G. A critical look at the kinetic

- parameter values used in simulating the thermoluminescence glow-curve[J]. Journal of Luminescence, 2017, **183**: 533 – 541. DOI: [10.1016/j.jlumin.2016.12.002](https://doi.org/10.1016/j.jlumin.2016.12.002).
- 16 Som S, Chowdhury M, Sharma S K. Kinetic parameters of γ -irradiated Y_2O_3 phosphors: effect of doping/codoping and heating rate[J]. Radiation Physics and Chemistry, 2015, **110**: 51 – 58. DOI: [10.1016/j.radphyschem.2015.01.015](https://doi.org/10.1016/j.radphyschem.2015.01.015).
- 17 Mishra G C, Verma U K, Singh R S, et al. Enhanced luminescence in co-doped $\text{LaCa}_4\text{O}(\text{BO}_3)_3$ phosphor: Photoluminescence, mechanoluminescence and thermoluminescence study[J]. Optik, 2022, **261**: 169112. DOI: [10.1016/j.ijleo.2022.169112](https://doi.org/10.1016/j.ijleo.2022.169112).
- 18 Tang W, Zuo C D, Li Y K, et al. Exploiting intervalence charge-transfer engineering to finely control $(\text{Ba}, \text{Sr})\text{TiO}_3$; Pr^{3+} luminescence thermometers[J]. Journal of Luminescence, 2021, **236**: 118103. DOI: [10.1016/j.jlumin.2021.118103](https://doi.org/10.1016/j.jlumin.2021.118103).
- 19 Donaldson J, Williams G V M. Photoluminescence, radioluminescence, and thermoluminescence in NaMgF_3 activated with Ni^{2+} and Er^{3+} [J]. Journal of Luminescence, 2016, **173**: 279 – 285. DOI: [10.1016/j.jlumin.2016.01.004](https://doi.org/10.1016/j.jlumin.2016.01.004).
- 20 Salah N, Sahare P D, Rupasov A A. Thermoluminescence of nanocrystalline $\text{LiF}: \text{Mg}, \text{Cu}, \text{P}$ [J]. Journal of Luminescence, 2007, **124**(2): 357 – 364. DOI: [10.1016/j.jlumin.2006.04.004](https://doi.org/10.1016/j.jlumin.2006.04.004).
- 21 Cooke D W, Hogstrom K R. Thermoluminescent response of LiF and $\text{Li}_2\text{B}_4\text{O}_7: \text{Mn}$ to pions[J]. Physics in Medicine and Biology, 1980, **25**(4): 657 – 666. DOI: [10.1088/0031-9155/25/4/004](https://doi.org/10.1088/0031-9155/25/4/004).
- 22 Petrenko M D, Ogorodnikov I N, Ivanov V Y. Thermoluminescence and low-temperature luminescence of beryllium oxide[J]. Radiation Measurements, 2016, **90**: 14 – 17. DOI: [10.1016/j.radmeas.2015.12.025](https://doi.org/10.1016/j.radmeas.2015.12.025).
- 23 Lakshmanan A R, Jose M T, Annalakshmi O. High-sensitive $\text{CaSO}_4: \text{Dy}$ thermoluminescent phosphor synthesis by co-precipitation technique[J]. Radiation Protection Dosimetry, 2008, **132**(1): 42 – 50. DOI: [10.1093/rpd/ncn215](https://doi.org/10.1093/rpd/ncn215).
- 24 Yazici A N, Chen R, Solak S, et al. The analysis of thermoluminescent glow peaks of $\text{CaF}_2: \text{Dy}$ (TLD-200) after-irradiation[J]. Journal of Physics D: Applied Physics, 2002, **35**(20): 2526 – 2535. DOI: [10.1088/0022-3727/35/20/311](https://doi.org/10.1088/0022-3727/35/20/311).
- 25 Ahmed M F, Schnell E, Ahmad S, et al. Image reconstruction algorithm for optically stimulated luminescence 2D dosimetry using laser-scanned Al_2O_3 ; C and $\text{Al}_2\text{O}_3: \text{C}, \text{Mg}$ films[J]. Physics in Medicine and Biology, 2016, **61**(20): 7484 – 7506. DOI: [10.1088/0031-9155/61/20/7484](https://doi.org/10.1088/0031-9155/61/20/7484).
- 26 Prokic M, Bøtter-Jensen L. Comparison of main thermoluminescent properties of some TL dosimeters[J]. Radiation Protection Dosimetry, 1993, **47**(1 – 4): 195 – 199. DOI: [10.1093/oxfordjournals.rpd.a081731](https://doi.org/10.1093/oxfordjournals.rpd.a081731).
- 27 Gavhane K H, Bhadane M S, Kulkarni P P, et al. Investigation of novel Eu doped SrDy_2O_4 microphosphor for thermoluminescence dosimetry[J]. Journal of Luminescence, 2021, **231**: 117781. DOI: [10.1016/j.jlumin.2020.117781](https://doi.org/10.1016/j.jlumin.2020.117781).
- 28 Sarıkçı S, Topaksu M, Bakr M, et al. Structural and analyses of thermoluminescence glow curves in Sm doped SrGd_2O_4 phosphor[J]. Journal of Alloys and Compounds, 2022, **911**: 165008. DOI: [10.1016/j.jallcom.2022.165008](https://doi.org/10.1016/j.jallcom.2022.165008).
- 29 Alajlani Y, Can N. Thermoluminescence glow curve analysis and kinetic parameters of Dy-doped BaSi_2O_5 phosphor[J]. Journal of Rare Earths, 2022, **40**(2): 234 – 242. DOI: [10.1016/j.jre.2020.10.020](https://doi.org/10.1016/j.jre.2020.10.020).
- 30 Zeng P, Wei X T, Yin M, et al. Investigation of the long afterglow mechanism in $\text{SrAl}_2\text{O}_4: \text{Eu}^{2+}/\text{Dy}^{3+}$ by optically stimulated luminescence and thermoluminescence[J]. Journal of Luminescence, 2018, **199**: 400 – 406. DOI: [10.1016/j.jlumin.2018.03.088](https://doi.org/10.1016/j.jlumin.2018.03.088).
- 31 Chernov V, Salas-Castillo P, Díaz-Torres L A, et al. Thermoluminescence and infrared stimulated luminescence in long persistent monoclinic $\text{SrAl}_2\text{O}_4: \text{Eu}^{2+}$, Dy^{3+} and $\text{SrAl}_2\text{O}_4: \text{Eu}^{2+}, \text{Nd}^{3+}$ phosphors[J]. Optical Materials, 2019, **92**: 46 – 52. DOI: [10.1016/j.optmat.2019.04.015](https://doi.org/10.1016/j.optmat.2019.04.015).
- 32 Manaka M C, Mothudi B M, Dhlamini M S. Photoluminescence and thermoluminescence properties of manganese doped BaAl_2O_4 phosphor[J]. Materials Science and Engineering: B, 2022, **278**: 115604. DOI: [10.1016/j.mseb.2022.115604](https://doi.org/10.1016/j.mseb.2022.115604).
- 33 Paikaray R, Badapanda T, Mohapatra H, et al. Investigation of structural, photoluminescence, and thermoluminescence properties of praseodymium doped CaWO_4 phosphor[J]. Materials Today Communications, 2022, **31**: 103802. DOI: [10.1016/j.mtcomm.2022.103802](https://doi.org/10.1016/j.mtcomm.2022.103802).
- 34 Reshes G, Eliyahu I, Oster L, et al. Comparison of optical absorption and thermoluminescence in $\text{LiF}: \text{Mg}, \text{Ti}$ (TLD-

- 100) following irradiation by high energy protons and ${}^{90}\text{Sr}/{}^{90}\text{Y}$ beta rays[J]. *Radiation Measurements*, 2020, **132**: 106249. DOI: [10.1016/j.radmeas.2020.106249](https://doi.org/10.1016/j.radmeas.2020.106249).
- 35 Som S, Chowdhury M, Sharma S K. Kinetic parameters of γ -irradiated Y_2O_3 phosphors: effect of doping/codoping and heating rate[J]. *Radiation Physics and Chemistry*, 2015, **110**: 51 – 58. DOI: [10.1016/j.radphyschem.2015.01.015](https://doi.org/10.1016/j.radphyschem.2015.01.015).
- 36 白小燕, 齐超, 金晓明, 等. 国产 $\text{LiF}(\text{Mg}, \text{Ti})\text{-M}$ 剂量片 γ 射线响应的线性上限和重复性研究[J]. *现代应用物理*, 2013, **4**(2): 152 – 156. DOI: [10.3969/j.issn.2095-6223.2013.02.010](https://doi.org/10.3969/j.issn.2095-6223.2013.02.010).
BAI Xiaoyan, QI Chao, JIN Xiaoming, et al. Linear upper limit and repeatability of thermoluminescence dosimeter of $\text{LiF}(\text{Mg}, \text{Ti})\text{-M}$ in γ -rays[J]. *Modern Applied Physics*, 2013, **4**(2): 152 – 156. DOI: [10.3969/j.issn.2095-6223.2013.02.010](https://doi.org/10.3969/j.issn.2095-6223.2013.02.010).
- 37 Zhao B, Hu S L, Wang D, et al. Inhibitory effect of gamma irradiation on *Penicillium digitatum* and its application in the preservation of Ponkan fruit[J]. *Scientia Horticulturae*, 2020, **272**: 109598. DOI: [10.1016/j.scienta.2020.109598](https://doi.org/10.1016/j.scienta.2020.109598).
- 38 Li F M, Gu Y B, Chen D H. Study on radiation preservation of frozen egg liquid[J]. *Radiation Physics and Chemistry*, 2000, **57**(3 – 6): 341 – 343. DOI: [10.1016/S0969-806X\(99\)00401-6](https://doi.org/10.1016/S0969-806X(99)00401-6).
- 39 Shannon R D. Revised effective ionic radii and systematic studies of interatomic distances in halides and chalcogenides[J]. *Acta Crystallographica Section A*, 1976, **32**(5): 751 – 767. DOI: [10.1107/s0567739476001551](https://doi.org/10.1107/s0567739476001551).
- 40 Jia Y Q. Crystal radii and effective ionic radii of the rare earth ions[J]. *Journal of Solid State Chemistry*, 1991, **95**(1): 184 – 187. DOI: [10.1016/0022-4596\(91\)90388-X](https://doi.org/10.1016/0022-4596(91)90388-X).
- 41 Huber G, Syassen K, Holzapfel W B. Pressure dependence of 4f levels in europium pentaphosphate up to 400 kbar[J]. *Physical Review B*, 1977, **15**(11): 5123 – 5128. DOI: [10.1103/physrevb.15.5123](https://doi.org/10.1103/physrevb.15.5123).
- 42 Lei B F, Li B, Zhang H R, et al. Synthesis and luminescence properties of cube-structured $\text{CaSnO}_3/\text{RE}^{3+}$ ($\text{RE}=\text{Pr, Tb}$) long-lasting phosphors[J]. *Journal of the Electrochemical Society*, 2007, **154**(7): H623. DOI: [10.1149/1.2734775](https://doi.org/10.1149/1.2734775).
- 43 Van den Eeckhout K, Bos A J J, Poelman D, et al. Revealing trap depth distributions in persistent phosphors [J]. *Physical Review B*, 2013, **87**(4): 045126. DOI: [10.1103/physrevb.87.045126](https://doi.org/10.1103/physrevb.87.045126).
- 44 郭竞渊, 唐强, 唐桦明, 等. LiMgPO_4 : Tm, Tb 的热释光和光释光陷阱参数[J]. *物理学报*, 2017, **66**(10): 313 – 319. DOI: [10.7498/aps.66.107802](https://doi.org/10.7498/aps.66.107802).
GUO Jingyuan, TANG Qiang, TANG Huaming, et al. Thermoluminescence and optical stimulated luminescence trap parameters of LiMgPO_4 : Tm, Tb [J]. *Acta Physica Sinica*, 2017, **66**(10): 313 – 319. DOI: [10.7498/aps.66.107802](https://doi.org/10.7498/aps.66.107802).
- 45 詹明亮, 陈瑶窈, 续卓, 等. 荧光粉 $\text{YGaAG: Ce}(\text{Y}_{2.96}\text{Ce}_{0.04}\text{Al}_{3.4}\text{Ga}_{1.6}\text{O}_{12})$ 的热释光研究[J]. *核技术*, 2020, **43**(5): 050501. DOI: [10.11889/j.0253-3219.2020.hjs.43.050501](https://doi.org/10.11889/j.0253-3219.2020.hjs.43.050501).
ZHAN Mingliang, CHEN Yaoya, XU Zhuo, et al. Investigation on thermoluminescence of phosphor $\text{YGaAG: Ce}(\text{Y}_{2.96}\text{Ce}_{0.04}\text{Al}_{3.4}\text{Ga}_{1.6}\text{O}_{12})$ [J]. *Nuclear Techniques*, 2020, **43**(5): 050501. DOI: [10.11889/j.0253-3219.2020.hjs.43.050501](https://doi.org/10.11889/j.0253-3219.2020.hjs.43.050501).
- 46 续卓, 郭竞渊, 熊正烨, 等. 掺 Tm^{3+} 和 Tb^{3+} 的 LiMgPO_4 磷光体的发光光谱与能量转移[J]. *物理学报*, 2021, **70**(16): 295 – 302. DOI: [10.7498/aps.70.20210357](https://doi.org/10.7498/aps.70.20210357).
XU Zhuo, GUO Jingyuan, XIONG Zhengye, et al. Luminescence spectra and energy transfer of Tm^{3+} and Tb^{3+} doped in LiMgPO_4 phosphors[J]. *Acta Physica Sinica*, 2021, **70**(16): 295 – 302. DOI: [10.7498/aps.70.20210357](https://doi.org/10.7498/aps.70.20210357).
- 47 McKeever S W S. *Thermoluminescence of solids*[M]. London: Cambridge University Press, 1988.
- 48 Xiong Z Y, Wang X C, Liang Y T, et al. Study of thermoluminescence, photoluminescence and dosimetry for the YAGG: $\text{Ce}(\text{Y}_{2.96}\text{Al}_{3.4}\text{Ga}_{1.6}\text{O}_{12}; 0.04\text{Ce})$ phosphor[J]. *Applied Radiation and Isotopes*, 2023, **193**: 110615. DOI: [10.1016/j.apradiso.2022.110615](https://doi.org/10.1016/j.apradiso.2022.110615).